Multiwinding High-Frequency Current Transformer for Power Cable Monitoring

Christoph Andres
Institute of Electric Power Systems
Otto von Guericke University
Magdeburg, Germany
christoph.andres@ovgu.de

Martin Fritsch
Institute of Electric Power Systems
Otto von Guericke University
Magdeburg, Germany
martin.fritsch@ovgu.de

Martin Wolter
Institute of Electric Power Systems
Otto von Guericke University
Magdeburg, Germany
martin.wolter@ovgu.de

***Abstract*—This paper investigates a multiwinding high-frequency current transformer (MWHFCT) designed for partial discharge (PD) detection on power cables. By extending a conventional high-frequency current transformer (HFCT) with additional windings, multifunctional applications such as energy harvesting become possible. To evaluate this concept, a simplified linear model of the MWHFCT is developed and validated through vector network analyzer (VNA) measurements, enabling analysis of how auxiliary windings affect the sensors transfer impedance. The results show that sensitivity remains largely unaffected when auxiliary windings are operated under open-circuit conditions and with a limited number of turns. Based on the analytical and experimental results, design guidelines are derived to ensure reliable PD detection and enable multifunctional, self-powered HFCTs for large-scale online power cable monitoring.**

***Index Terms*—Current transformers, high-frequency, multi-winding, partial discharges (PD), power cables, scattering (S) parameters, transfer impedance**

I. Introduction

Power cables are an essential component of power grids worldwide. To prevent failures and enable future large-scale online monitoring, the partial discharge (PD) activity of these assets can be measured. Internal PDs are an indicator of the condition of the cable insulation and generate high-frequency current pulses that propagate as traveling waves along the cable [1]. High-frequency current transformers (HFCTs) can be used to detect these transient signals. An HFCT consists mainly of a ferromagnetic core and a secondary winding in which a voltage is induced. The operating principle is described in detail in [2]–[4].

For large-scale online monitoring, numerous HFCTs will be needed. From an economic perspective, it is therefore advantageous if these sensors can perform additional functions beyond PD detection. Examples include providing electrical energy through inductive energy harvesting, as described in [5], [6], as well as obtaining additional electrical parameters of the grid, such as power quality indicators (see e.g., [7]) and the 50 Hz-component of the power cable current. Such a sensor would be a multifunctional and self-powered HFCT.

A so-called multiwinding HFCT (MWHFCT) can be used for this purpose. In addition to the main winding for PD detection, they have auxiliary windings on the same core that can be used for other functions, see Fig 1. However, these auxiliary windings must not negatively influence each other. In particular, the parasitic capacitances and inductances of the additional windings and their loading can influence the transmission behavior of the HFCT.

Previous research has primarily focused on conventional HFCTs with a single PD measurement winding. Approaches extending such conventional HFCTs by additional windings have rarely been investigated, especially in the context of PD detection. Therefore, this paper investigates the fundamental principles of extending a conventional HFCT for PD detection on power cables into a MWHFCT.

The main contributions of this paper are as follows:

- Development and validation of a linear model of a MWHFCT in the frequency domain
- Experimental investigation of the influence of additional windings on the frequency-dependent transfer impedance of the PD measurement winding
- Derivation of design guidelines for an MWHFCT intended for PD detection on power cables

The paper is organized as follows: Section II presents the MWHFCT model. Section III describes the measurement of the transfer impedance with subsequent model validation. Section IV discusses the measurement results, and Section V concludes the paper.

II. Linear Model of the Multiwinding High-Frequency Current Transformer

The basic operating principle of a MWHFCT is illustrated in Fig. 1. Several secondary windings (n_2, ... ,n_n) are wound on a ferromagnetic core that encloses the inner conductor of a power cable. The primary current $i_1(t)$ through this conductor is the superposition of the 50 Hz operating current, high-frequency PD signals, and noise. It generates a magnetic flux density $B(t)$ in the core, which in turn induces voltages ($u_2(t)$, ... ,$u_\mathrm{n}(t)$) in the secondary windings.

In this work, the winding n_2 is the measurement winding for PD detection. The induced voltage $u_2(t)$ will therefore be used to measure the high-frequency current pulses. The auxiliary windings n_k, ... ,n_n can be utilized for different purposes as described in Section I. As with all current transformers, the primary winding has a single turn, $n_1 = 1$. It can therefore be concluded that the MWHFCT, just like a conventional HFCT,

979-8-3315-8138-1

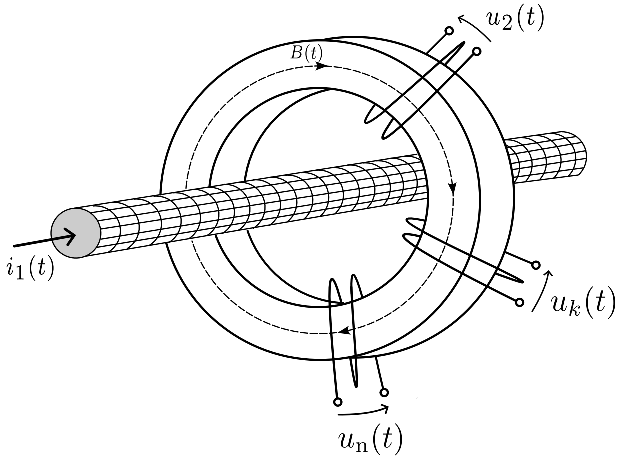

Fig. 1. Basic structure and operating principle of a MWHFCT.

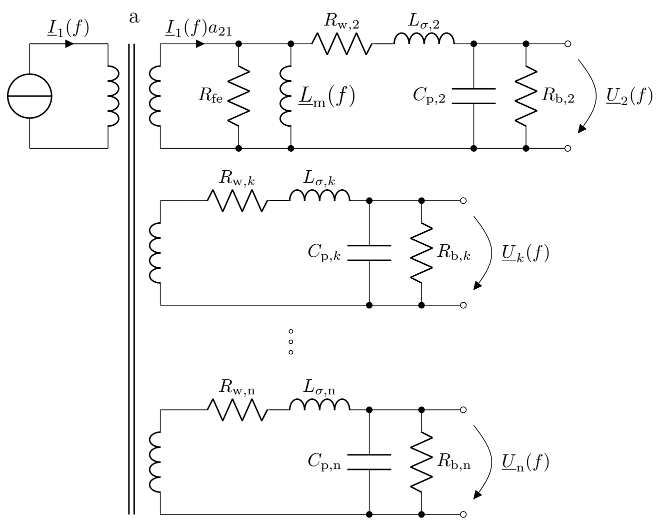

Fig. 2. EQC of a MWHFCT without interwinding capacitances between the windings n_1, ... ,n_n.

operates according to the transformer principle. However, instead of one, it has several winding ratios a:

$$a_{21} = \frac{n_1}{n_2},\ a_{2k} = \frac{n_k}{n_2},\ a_{2\mathrm{n}} = \frac{n_\mathrm{n}}{n_2}. \tag{1}$$

If the core material of the MWHFCT is not saturated, a complex, frequency-dependent but linear permeability can be assumed [2]:

$$\underline{\mu}_\mathrm{c}(f) = \mu'(f) - \mathrm{j}\mu''(f). \tag{2}$$

How saturation in HFCTs can be avoided is discussed in [8]. The use of linear permeability allows linear modeling of the MWHFCT in the frequency domain, which is carried out in the following two subchapters.

A. General Equivalent Circuit Model

Fig. 2 shows the general and linear equivalent circuit (EQC) in the frequency domain, which neglects the capacitive couplings between the windings n_1, ... ,n_n (interwinding capacitances). The magnetic flux in the core is represented by the magnetization inductance $\underline{L}_\mathrm{m}(f)$, which is approximately:

$$\underline{L}_\mathrm{m}(f) \approx \frac{n_2^2 \mu_0 \underline{\mu}_\mathrm{c}(f) A_\mathrm{c}}{2\pi r_\mathrm{c,m}}. \tag{3}$$

The vacuum permeability is $\mu_0 \approx 1.25664 \cdot 10^{-6}\,\frac{\mathrm{Vs}}{\mathrm{Am}}$. Here, A_c denotes the core cross-sectional area, and $r_\mathrm{c,m}$ is the mean core radius. The resistance of the copper winding can be described by R_w. Core losses due to hysteresis and eddy currents are represented by R_fe. The shown leakage flux L_σ describes the imperfect magnetic coupling and the parasitic capacitance C_p the turn-to-turn electric field coupling of each winding.

To facilitate further analysis based on the presented model, a simplified EQC is derived in the following subsection.

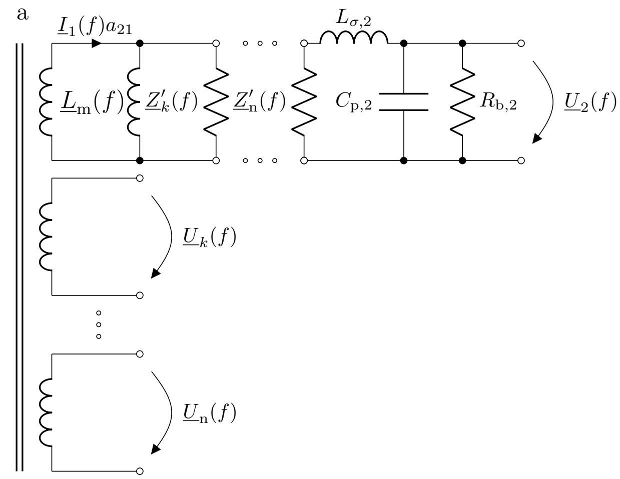

Fig. 3. Simplified EQC of a MWHFCT. The impedances of the additional windings n_k, ... ,n_n are referred to the PD measuring winding n_2. As with the more general model, interwinding capacitances are not taken into account.

B. Simplified Equivalent Circuit Model

For the MWHFCT model shown, some assumptions and simplifications can be made to reduce the complexity of the EQC. The hysteresis loss in ferrite materials is represented by the imaginary part of the complex permeability μ'', which is already included in $\underline{L}_\mathrm{m}(f)$. Due to the low electrical conductivity of the material, eddy current losses remain very small even at high frequencies. Consequently, when ferrite toroids are used as core, the resistance R_fe can be neglected [2]. Furthermore, for the PD measuring winding of an HFCT, the number of turns is usually $n_2 \leq 5$, and therefore the winding resistance $R_\mathrm{w,2}$ can be neglected [2]. The resulting simplified EQC is shown in Fig. 3. The impedance of the PD measuring winding resulting from the assumptions made can be determined via:

$$\underline{Z}_2(f) = \frac{1}{\frac{1}{R_\mathrm{b,2}} + \mathrm{j}\omega C_\mathrm{p,2}} + \mathrm{j}\omega L_{\sigma,2}. \tag{4}$$

Similarly, the magnetization inductance can be calculated as frequency-dependent impedance:

$$\underline{Z}_\mathrm{m}(f) = \mathrm{j}\omega \underline{L}_\mathrm{m}(f). \tag{5}$$

979-8-3315-8138-1

For further simplification, the circuit components belonging to each additional winding are combined into an individual total impedance $\underline{Z}_k(f)$. Each of these impedances is then referred to the PD measuring winding n_2 as follows:

$$\underline{Z}_k'(f) = \frac{1}{a_{2k}^2}\underline{Z}_k(f) \tag{6}$$

where each impedance $\underline{Z}_k(f)$ is calculated as:

$$\underline{Z}_k(f) = \frac{1}{\frac{1}{R_{\mathrm{b},k}} + \mathrm{j}\omega C_{\mathrm{p},k}} + (R_{\mathrm{w},k} + \mathrm{j}\omega L_{\sigma,k})\,. \tag{7}$$

For further calculations, the previously introduced impedances are combined into the total impedance of the winding n_2:

$$\underline{Z}_{\mathrm{tot}}(f) = \left(\frac{1}{\underline{Z}_{\mathrm{m}}(f)} + \sum_{k=3}^{\mathrm{n}} \frac{1}{\underline{Z}_k'(f)} + \frac{1}{\underline{Z}_2(f)}\right)^{-1}. \tag{8}$$

This total impedance can now be used to determine the transfer impedance $\underline{Z}_{\mathrm{T}}(f)$ of the MWHFCT, which is representative of the sensitivity of the PD measuring winding n_2. It is defined as the ratio of the primary current $\underline{I}_1(f)$ to the output voltage $\underline{U}_2(f)$ [2]:

$$\underline{Z}_{\mathrm{T}}(f) = \frac{\underline{U}_2(f)}{\underline{I}_1(f)} \tag{9}$$

where the induced voltage $\underline{U}_2(f)$ for a MWHFCT is given by:

$$\underline{U}_2(f) = \frac{\left(\frac{1}{R_{\mathrm{b},2}} + \mathrm{j}\omega C_{\mathrm{p},2}\right)^{-1} \underline{Z}_{\mathrm{tot}}(f)}{\left(\frac{1}{R_{\mathrm{b},2}} + \mathrm{j}\omega C_{\mathrm{p},2}\right)^{-1} + \mathrm{j}\omega L_{\sigma,2}} \underline{I}_1(f) a_{21}. \tag{10}$$

The interwinding capacitances as well as the parasitic capacitances C_{p} and leakage inductances L_σ of the proposed EQC are difficult to determine, both experimentally and analytically. Since these parameters are not yet known, they are neglected in the subsequent analyses. The authors plan to present a more complete model of the MWHFCT in a future publication.

To enable experimental validation of the developed model, Section III presents a measurement method for determining the transfer impedance.

III. Measurement of the Transfer Impedance

For the measurement of the transfer impedance $\underline{Z}_{\mathrm{T}}(f)$, a HFCT optimized for PD detection is used, which was developed and described in detail in [2]. Since this sensor was developed for online monitoring of power cables, it is designed for a measurement bandwidth of $f < 10\,\mathrm{MHz}$ [2]. The toroidal ferromagnetic core used is manufactured by Fair-Rite and consists of material type No. 43 (nickel-zinc). The core dimensions are 31.75 x 51.30 x 15.90 mm ($r_{\mathrm{c,in}}$ x $r_{\mathrm{c,out}}$ x h_{c}).

The PD measurement winding comprises $n_2 = 3$ turns and is terminated with a load resistor $R_{\mathrm{b},2} = 50\,\Omega$. These parameters ensure high sensitivity and remain constant for all subsequent analyses. For this work, the described HFCT is extended to a MWHFCT by adding additional windings n_k, ... ,n_{n} with different load resistors $R_{\mathrm{b},k}$, ... ,$R_{\mathrm{b,n}}$. For this purpose, the resistors are soldered to the ends of the windings. All windings

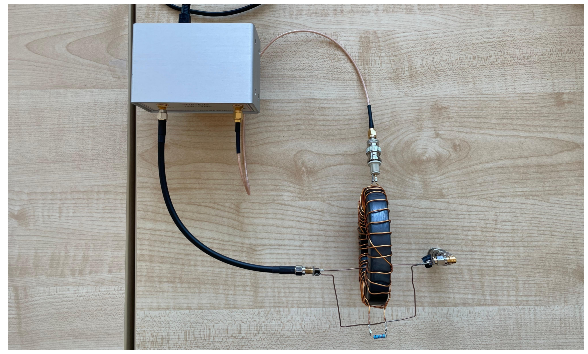

Fig. 4. Measurement setup for determining the transfer impedance. The MWHFCT is connected to the TX and RX ports of the VNA via two coaxial cables in order to measure the complex S-parameters $\underline{S}_{21}(f)$ and $\underline{S}_{11}(f)$.

are uniformly wound around the core to minimize parasitic coupling effects.

To determine the transfer impedance of the MWHFCT, a vector network analyzer (VNA) was employed. The VNA measures the scattering parameters (S-parameters) of a linear two-port network, which provide information about the frequency-dependent transfer behavior of the sensor. The *DG8SAQ VNWA 3E* from SDR-Kits is used as the measurement device. The measurement setup is shown in Fig. 4.

As can be seen, the MWHFCT is connected to the VNA via two ports. The transmit (TX) output of the VNA is connected to the adapter through the black coaxial cable. Since the adapter separates the forward and return conductors, signal coupling into the MWHFCT is enabled. The adapter is terminated with an SMA impedance $Z_{11} = 48.43\,\Omega$. The receive (RX) input of the VNA is connected via the bright coaxial cable to the PD measurement output of the MWHFCT, which corresponds to the terminals of the PD measuring winding n_2.

To ensure that the measurement is not influenced by setup components (e.g., cables, connectors, or adapters), the system was calibrated prior to measurement. The Short-Open-Load-Through (SOLT) method is used for calibration and implemented with the VNA software. Further details on the calibration procedure can be found in [2].

After successful calibration, the complex S-parameters $\underline{S}_{11}(f)$ and $\underline{S}_{21}(f)$ are measured, from which the absolute value of the transfer impedance $|\underline{Z}_{\mathrm{T}}(f)|$ can be calculated as follows:

$$|\underline{Z}_{\mathrm{T}}(f)| = \left|\frac{\underline{S}_{21}(f) \cdot Z_{11}}{1 - \underline{S}_{11}(f)}\right|. \tag{11}$$

The measurement range was set from 0.1 to 60 MHz to capture the full transfer behavior of the MWHFCT. Considering that PD signals usually contain significant frequency components below 10 MHz [9], only this range is evaluated in the subsequent analysis.

For the validation of the developed model, the measured values of the transfer impedance of the MWHFCT are compared with the values predicted by the model. The validation results are shown in Fig. 5.

979-8-3315-8138-1

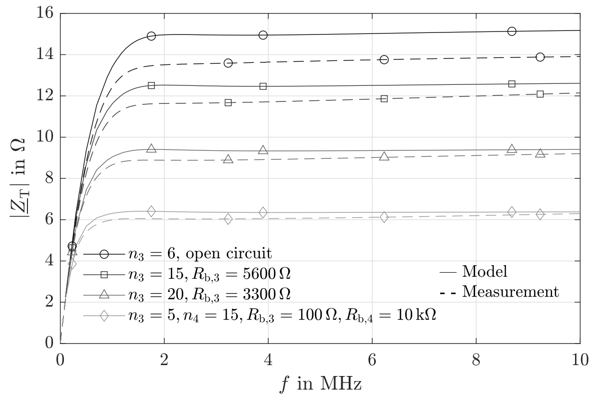

Fig. 5. Measured transfer impedance of the MWHFCT compared with the results of the simplified analytical model.

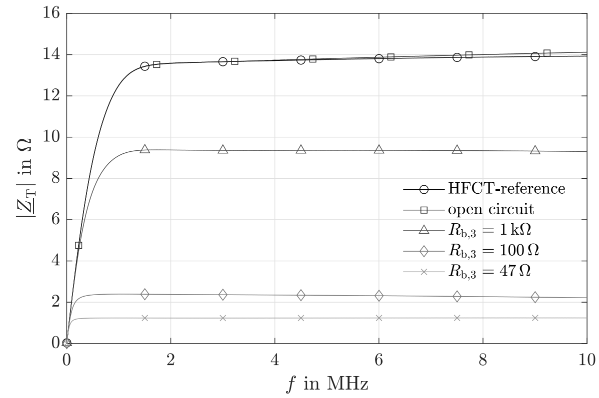

Fig. 6. Influence of the load resistance $R_{\mathrm{b},3}$ of an additional winding n_3 on the transfer impedance. The number of turns is constant at $n_3 = 10$.

Four different scenarios can be distinguished, corresponding to different configurations of the MWHFCT. As can be seen, the model agrees well with the measured transfer impedance values. The transfer function of the MWHFCT in the frequency range under consideration is similar to that of a high-pass in all four cases, which is also typical for a conventional HFCT. The magnitude of the transfer impedance increases approximately linearly with frequency at low frequencies, reaches a transition at the cutoff frequency, and exhibits a nearly flat frequency response at higher frequencies up to 10 MHz. The flat frequency response ensures that the signals are not distorted by the measurement.

The largest deviation between measurement and model occurs for the configuration $n_3 = 6$ in the open-circuit condition, with an average percentage deviation of $\approx 6\,\%$. This deviation is comparable to the model error reported in [2] and occurs in the configuration where parasitic effects are least suppressed. In the open-circuit condition, both the leakage inductance L_σ and the parasitic capacitance C_p have a stronger influence, which leads to a larger deviation in the simplified model.

Since a simplified model is used, in which all parasitic elements (including interwinding capacitances) are neglected, the model is not universally applicable to all MWHFCT configurations (e.g. high number of turns of additional windings). Under certain conditions, parasitic effects can have a significant impact on the transfer function of the MWHFCT (see Subsection IV-B). For a complete model, a method would be required to accurately determine these parasitic parameters, which was not possible for the authors at this stage.

The next Section IV presents the analysis of the measured results. Here, the influence of additional windings on the transfer impedance is evaluated.

IV. Influence of Additional Windings on Sensitivity

Since PD typically appear as very short current pulses with low amplitude at the end of a power cable, highly sensitive sensors are required for their detection. When extending a HFCT to a MWHFCT, it must be ensured that the sensor sensitivity is not degraded. This implies that the transfer impedance within the relevant frequency range up to 10 MHz should remain as unaffected as possible.

In the following analyses, a HFCT reference scenario is therefore used, representing the frequency-dependent transfer function of an HFCT without additional windings as a benchmark for comparison. All transfer impedance characteristics discussed are based on measured data, allowing the verification of how an MWHFCT can be designed without compromising the functionality or sensitivity of the sensor.

A. Load Resistance

Fig. 6 illustrates the influence of the load resistance of additional windings on the transfer impedance of the MWHFCT.

The number of turns of a single auxiliary winding is constant $n_3 = 10$, while the load resistance $R_{\mathrm{b},3}$ varies. It can clearly be seen that a decreasing load resistance has a negative impact on the sensitivity of the PD measuring winding. As the load resistance decreases, the flat plateau of the transfer impedance shifts towards lower values, resulting in a reduced sensitivity in the relevant frequency range. However, if there is an open-circuit ($R_{\mathrm{b},3} \to \infty$), the transfer impedance of the MWHFCT remains almost the same as for the HFCT reference scenario.

This effect can be explained by the fact that a lower load resistance causes a stronger influence on the magnetic flux within the core. The resulting flux compensation leads to a reduction of the induced voltage $\underline{U}_2(f)$. For PD detection applications, this means that additional windings are only permissible if they operate under open-circuit or near open-circuit conditions to avoid degrading the sensitivity of the PD measuring winding.

Further analysis show that it is not only the absolute value of the load resistance that is crucial, but also the ratio between the number of turns and the load resistance $n_k/R_{\mathrm{b},k}$. If the number of turns is increased at a constant load resistance, the transfer impedance decreases and with it the sensitivity of the PD measuring winding. In addition, it can be seen that, with several additional windings, the winding with the higher

979-8-3315-8138-1

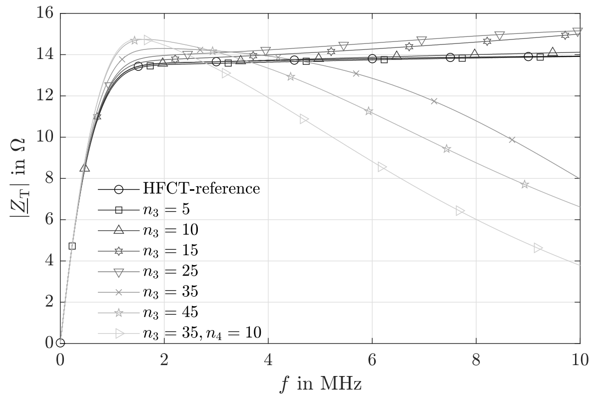

Fig. 7. Influence of the number of turns of additional windings under open-circuit conditions on the transfer impedance $|\underline{Z}_\mathrm{T}(f)|$.

number of turns always has the dominant influence on the flux in the core.

It can therefore be concluded that an additional winding, which cannot be operated in open-circuit due to its function, must not be active in parallel with the PD measurement. This includes, for example, the winding that can be used for energy decoupling. The two techniques, PD measurement and decoupling of energy, would therefore have to be carried out alternately. Furthermore, it can be concluded that an active additional winding to prevent saturation in HFCTs is not applicable for PD detection. This confirms the strategy proposed in [8] for preventing saturation by using a air gap control. For applications in which the additional winding is operated in open-circuit condition, such as for measuring other electrical quantities, simultaneous operation is not critical.

B. Number of Turns

Fig. 7 illustrates the influence of the number of turns of the additional passive windings (open-circuit conditon) on the transfer impedance $|\underline{Z}_\mathrm{T}(f)|$ of the MWHFCT.

It can be seen that, for small numbers of turns, the transfer impedance is almost identical to the HFCT reference scenario. However, it can be observed that the influence increases with a higher number of turns. At $n_3 > 25$, a noticeable distortion of the originally flat frequency response can be seen in the range of 1 to 10 MHz. These distortions can reduce the accuracy and reliability of PD pulse detection.

This behavior can be explained by parasitic elements such as leakage inductances L_σ, parasitic capacitances C_p and inter-winding capacitances. Increasing both the number of windings on the ferromagnetic core and the number of turns per winding increases these parasitic effects. These results suggest that even passive auxiliary windings can significantly influence the frequency response of the sensor if their number of turns is too high. When designing an MWHFCT, it is therefore essential to take into account the parasitic effects.

The number of auxiliary windings and their respective number of turns should therefore be kept as low as possible. If a higher number of turns is required, e.g. for energy harvesting applications, additional design measures must be taken. These include optimized winding geometry and sufficient spacing between the individual turns. Reducing the load resistances of the additional windings can partially reduce parasitic effects, but at the same time leads to a significant reduction of the transfer function and thus to reduced sensitivity for PD detection of the MWHFCT.

V. Conclusion

In this paper, a simplified linear model of a MWHFCT for PD detection was presented and experimentally validated using VNA measurements. Further experimental results show that the load resistance and number of turns of the auxiliary windings have a significant impact on the original transfer impedance. A lower load resistance reduces the sensitivity of the PD measuring winding, while a higher number of turns increases parasitic effects and leads to distortion in the relevant frequency range. When auxiliary windings are operated under open-circuit conditions and have only a small number of turns, the transfer impedance remains nearly constant, preserving the sensors ability to reliably detect PD activity.

The presented model neglects interwinding capacitances and it was not possible to determine the other parasitic parameters of the MWHFCT. Thus the validity of the proposed model is limited to configurations with small number of the turns of the auxilary windings. Future work will focus on developing a more complete model including all parasitic elements, establishing measurement procedures for their determination, analyzing the coupling behavior between windings in greater detail, and identifying design measures to mitigate parasitic effects.

References

[1] S. Boggs and J. Densley, "Fundamentals of partial discharge in the context of field cable testing," *IEEE Electrical Insulation Magazine*, vol. 16, no. 5, pp. 13–18, Sep. 2000.

[2] M. Fritsch and M. Wolter, "High-frequency current transformer design and construction guide," *IEEE Transactions on Instrumentation and Measurement*, vol. 71, pp. 1–9, 2022.

[3] C. Zachariades, R. Shuttleworth, R. Giussani, and R. MacKinlay, "Optimization of a high-frequency current transformer sensor for partial discharge detection using finite-element analysis," *IEEE Sensors Journal*, vol. 16, no. 20, pp. 7526–7533, Oct. 2016.

[4] J. V. Kluss, A.-P. Elg, and C. Wingqvist, "High-frequency current transformer design and implementation considerations for wideband partial discharge applications," *IEEE Transactions on Instrumentation and Measurement*, vol. 70, pp. 1–9, 2021.

[5] C. Andres, M. Fritsch, and M. Wolter, "Inductive energy harvester with saturation-controlled maximum power point tracking," in *2024 IEEE Power and Energy Society General Meeting (PESGM)*. IEEE, Jul. 2024, pp. 1–5.

[6] J. Moon, J. Donnal, J. Paris, and S. B. Leeb, "VAMPIRE: A magnetically self-powered sensor node capable of wireless transmission," in *2013 Twenty-Eighth Annual IEEE Applied Power Electronics Conference and Exposition (APEC)*. IEEE, mar 2013.

[7] B. A. Siddiqui, P. Pakonen, and P. Verho, "Novel inductive sensor solutions for on-line partial discharge and power quality monitoring," *IEEE Transactions on Dielectrics and Electrical Insulation*, vol. 24, no. 1, pp. 209–216, Feb. 2017.

[8] M. Fritsch and M. Wolter, "High-frequency current transformer with variable air gap for power cable monitoring," *IEEE Transactions on Instrumentation and Measurement*, vol. 73, pp. 1–10, 2024.

[9] ——, "Measurable bandwidth of partial discharges on medium voltage cables," in *2021 IEEE Power and Energy Society General Meeting (PESGM)*. IEEE, Jul. 2021, pp. 1–5.